Heliyon 9 (2023) e21727

Contents lists available at ScienceDirect

Heliyon

journal homepage: www.cell.com/heliyon

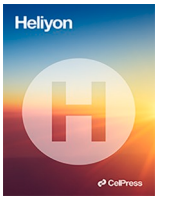

Dynamics of chemically reactive Carreau nanomaterial flow along a stretching Riga plate with active bio-mixers and Arrhenius catalysts

Saiful Islam [a], B.M.J. Rana [b], Md Shohel Parvez [c], Md Shahadat Hossain [b], Malati Mazumder [d], Kanak Chandra Roy [d], M.M. Rahman [a,*]

[a] Department of Mathematics, Bangladesh University of Engineering and Technology, Dhaka, Bangladesh
[b] Department of Quantitative Sciences, International University of Business Agriculture and Technology, Dhaka, Bangladesh
[c] Physics Discipline, Khulna University, Khulna, Bangladesh
[d] Department of Applied Mathematics, Gono Bishwabidyalay, Dhaka, Bangladesh

ARTICLE INFO

Keywords:
Nanofluid
Carreau fluid
Bio-convection
Magnetohydrodynamic
Activation energy
Riga plate
Finite difference method

ABSTRACT

Nanomaterial flow has fascinated the concern of scientists across the globe due to its innovative applications in various manufacturing, industrial, and engineering domains. Bearing aforementioned uses in mind, the focal point of this study is to examine the Carreau nanofluid flow configured by the Riga surface with Arrhenius catalysts. Microorganisms are also suspended in nanofluid to strengthen the density of the regular fluid. Time-dependent coupled partial differential equations that represent the flow dynamics are modified into dimensionless patterns via appropriate non-dimensional variables, and handled through an explicit finite difference approach with stability appraisal. The performances of multiple flow variables are examined graphically and numerically. Representation of 3D surface and contour plots for heat transportation and entropy generation are also epitomized. The findings express that the modified Hartmann number strengthens the motion of nanomaterial. Reverse outcomes for heat transport rate and entropy are seen for the radiation variable. Concentration diminishes for chemical reaction variable. Activation energy enhances the concentration of nanomaterial, whereas reduction happens in the movement of microbes for bio-Lewis number. Greater Brinkman variable heightens the entropy.

1. Introduction

The up-to-date spotlight of scientific and engineering research is nanomaterial flow. The expansion of heat transmission rates in industrial processes such as heat exchangers, electronic device cooling, microelectronics, fusion reactors, computer processors, mineral oils, cooling of nuclear reactors, cooling of transformer etc., is made conceivable by this noteworthy scientific spectacle. They have some biomedical and pharmaceutical applications such as the treatment of cancer, particular drug transport, antimicrobial

* Corresponding author.
E-mail addresses: saiful.islam@stamforduniversity.edu.bd (S. Islam), jewel.math@iubat.edu (B.M.J. Rana), shohel.ku.phy@ku.ac.bd (M.S. Parvez), shahadat_qs@iubat.edu (M.S. Hossain), malati.amath@gonouniversity.edu.bd (M. Mazumder), kanak.amath@gonouniversity.edu.bd (K.C. Roy), mmustafizurrahman@math.buet.ac.bd (M.M. Rahman).

https://doi.org/10.1016/j.heliyon.2023.e21727
Received 22 March 2023; Received in revised form 20 October 2023; Accepted 26 October 2023
Available online 28 October 2023

agents, and regenerative medicine. A nanofluid is an appropriate suspension of conventional liquids with nanometer-sized solid particles. The first effort on nanofluids was carried out by Choi [1] with a declaration that the insertion of nanoparticles into conventional fluids improves their thermal performance. Moreover, to augment the thermal enactment of common liquids, Buongiorno et al. [2] offered another scientific model for a nanofluid. Khan and Pop [3] described the thermophoresis and random motion in boundary layer nanofluid flow towards a stretching sheet. Time-dependent radiative nanofluid flow with thermophoresis and random movement feature was scrutinized by Khan et al. [4]. Makinde et al. [5] discussed the combined outcomes of random motion and thermo-migration on electric conductive nanofluid towards a stretchy sheet with a magnetic field. Further, numerous research works were carried out on the nanofluid flow problem [6–12] to regulate the heat transfer mechanisms in various systems.

Diversified manufacturing materials including polymers, emulsions, blood, medicine production, silicon oils, printer ink, shampoos, gypsum paste, foams, and toothpaste do not satisfy Newton's law of viscosity. Such kind of materials demonstration nonlinear relationships between shear rate and shear stress, and are recognized as non-Newtonian fluids. To describe the rheology of these materials, multiple models are addressed. Among them, the Carreau fluid model, developed by Carreau [13], is one of the most well-known models which describes shear thickening and thinning features at high and squat shear rates. Such a model precisely forecasts how polymer suspension operates in all manner of fluid problems. A few examples of Carreau fluids are animal blood, molten polymers, pulps, and toothpaste. This fluid has gotten a lot of interest because of its importance in tumor treatment, polymer extrusion, cosmetics, bitumen for road building, and so on.

For instance, Hayat et al. [14] studied Carreau nanomaterial flow over stretched surfaces with thermophoresis and random motion effects. Significant research on 2D Carreau fluid flow above stretched surfaces was scrutinized by Khan et al. [15] who included MHD which reduced the fluid velocity. Magnetized radiative Carreau nanofluid flow on stretched surfaces for both shear thickening and thinning issues was investigated by Waqas et al. [16]. Eid et al. [17] carried out a numerical study about Carreau nanofluid across a porous nonlinear stretching surface. They included the thermal radiation effect, which diminished heat transfer rate, and injection/suction. On a stretching sheet, Abbas et al. [18] explored mixed convective second-grade nanofluid including the non-linear thermal radiation effect. Various investigators have used Carreau fluid model [19–22] to interpret the physical behaviors of non-Newtonian fluid.

Bioconvections have gained the concentration of investigators in modern times due to their groundbreaking applicability in industrial and biological processes. Such a phenomenon arises due to the motion of swimming microorganisms. Gyrotactic microorganisms are a type of living thing that can swim on their own when stimulated by external factors such as gravity, light intensity, oxygen, and chemical gradient. Such a significant phenomenon has revolutionary uses in the sciences and engineering domains including protein production, biosensors, bioreactors, biodiesel, bio-fertilizers, cell treatment, and drug delivery [23–28]. Also, the density of these gyrotactic microorganisms is a little denser than water. Gyrotactic microorganisms tend to concentrate at the fluid layer's top portion due to up-swimming, which results in a top-heavy density stratification. Due to Brownian motion, the nanoparticle along this fluid domain gets motion, and the movement of motile microorganisms is independent of the movement of nanoparticles. The combined dynamics of nanoparticles and microorganisms play a significant role in microfluidic devices and micro-reactors [29]. Rana et al. [30] described how swimming bacteria impact the motion of human blood flow including nanoparticles. To investigate the nature of thermodynamic and mass transfer, Nisar et al. [31] included gyrotactic micro-organisms on the Carreau-Yasuda nanofluid with magnetic effect. Furthermore, Waqas et al. [32] analyzed magnetized micropolar nanofluid including the motion of gyrotactic microorganisms and variable thermal conductivity. Further, Carreau nanofluid flow with the activity of swimming microbes over a stretching sheet was discussed by Muntazir et al. [33].

The Riga plate is known as an electromagnetic actuator that has distinct industrial uses in geophysics, engineering, and astrophysics. Some applications of such electrical plates are micro-coolers, submarines, and thermal reactors [34]. The flow of weakly conductive fluid from an actuator with the integration of two things, magnetic and electric fields, formed a Riga plate, which was first designed by Gailitis et al. [35]. It is constructed with the combination of a spanwise arranged array of interchanging stable electrodes and magnets. Such an electrical plate produces a surface parallel force that decays exponentially normally to the plate. Hayat et al. [36] discussed the behaviors of random motion and thermophoresis on heated Riga plates. Mass and thermal transportation of nanofluid towards stretched Riga plate was reported by Vaidya et al. [37]. Moreover, Rooman et al. [38] analyzed Williamson nanofluid including MHD above an upright Riga plate. Variable heat conductivity and nonlinear thermal radiation were also considered. Loganathan et al. [39] used a Riga plate to describe the dynamics of Casson fluid with radiation and chemical reaction impacts. Bhatti et al. [40] discussed the significance of bioconvection with Arrhenius catalysts over a Riga plate which covered by microorganisms and nanofluid.

Activation energy has been turned into a hot topic of research for the past few years due to its applicability in engineering and manufacturing processes including oil reservoir engineering, food processing, mechanical chemistry, multiple suspensions of emulsions, chemical engineering, and geothermal reservoirs. Activation energy is referred to as the minimal quantity of energy needed to initiate a particular chemical response. Arrhenius pioneered the theory of activation energy. Various investigators examined how activation energy is performed in several flow situations. Afterward, Shi et al. [41] explored the consequence of activation energy for bioconvective Cross-nanofluid over a stretching seeming. Hussain et al. [42] discussed the behavior of activation energy on Carreau fluid flow with the belongings of Brownian and thermophoresis motion. Lately, dynamics of microorganisms on Carreau nanofluid with activation energy have been conducted by Shahid et al. [43]. Rana et al. [44] discussed the behaviors of Arrhenius catalysts with the measurement of entropy production. The theology of entropy is used to confirm the efficiency of any system in engineering and industrial appliances. Measurement of entropy production is operated to promote the system performance. Fluid friction, mass transport, heat transport, magnetic field, and diffusion can be regarded as the sources of entropy production. Various efforts towards the aspect of entropy production in multiple systems have been measured by several researchers [45–50]. The rest of the sections are

organized as the schematic representation of this model is specified in section 2, the mathematical archetypal to calculate the entropy is described in section 3, the solution methodology is explained in section 4, result comparison with previously published work is discussed in section 5, and the discussion of the results about the involved factor on fluid flow and heat transfer rate is described in section 6.

1.1. Motivation

The aforesaid analyses offered motivation for the investigation of Arrhenius catalysts in Carreau fluid flow with bacteria, due to their tremendous applicability in chemical, pharmaceutical, and manufacturing industries. Surface active molecules and surfactants are produced from microorganisms. Surfactants are utilized in the domains of multiple environmental bioremediation and enhanced oil recovery. Additionally, the Carreau fluid model can illustrate the rheological behaviors of shear thinning and thickening fluids. Some useful examples of the Carreau nanofluid model are thermonuclear warehouses, microelectronics, surgical diligence, and mechanical networks. Entropy generation of Carreau fluid model, when the flow is time-dependent and produced from a Riga sheet with bacteria, has not been explored earlier. Therefore, the ongoing study focusses on the scrutinization of entropy production and heat transfer operation in a Riga plate with nano-bio-mixers. Active bacteria are suspended in diluted Carreau nanomaterial. The regulatory flow problem is tackled through an explicit finite difference approach [51,52]. Achieved results are validated with earlier studies. Behaviors of physical parameters are described via graphs and Tables. This model will be helpful in the design of various thermal and engineering appliances.

1.2. Novelty

The originality and novelty of the present experiment are that the finite difference tool is applied to organize a numerical solution for unsteady Carreau nanomaterial flow of mass and heat transfer produced from stretchy Riga plate with Arrhenius catalysts, chemical reaction, random motion, and thermo-migration impacts. One of our novelties is the representation of 3D surface plots and contour plots for heat transportation and entropy production in radiative nanofluids. The novel outcomes offer a better perception of the flow characteristics of chemically reactive Carreau fluid and heat transportation in the presence of bacteria and Arrhenius catalysts, which will be helpful in multiple engineering and manufacturing applications such as bio-fuels, bio-fertilizers, mechanical networks, and geophysics.

2. Problem development

Here dynamics of two-dimensional incompressible Carreau nanofluid through a Riga plate are regarded. The flow of fluid is time-dependent and originated from a stretchy sheet. Biomolecules of microbes are suspended into nanofluid, to improve the stability and reliability problems of nanomaterials. Diluted suspensions of nano-molecules and biomolecules are regarded here. The Buongiorno sculpture is taken into account to characterize the attributes of nano-molecules properly. To describe the mass transportation mechanism, chemical reaction and the Arrhenius activation energy are adopted. A coordinate system initiates from the initial side of Riga plate.

The velocity is represented by (u, v) in (x, y) direction where x is directed lengthwise and y behaves normally to the sheet. The stretching motion of the sheet is $u = U_0 = ax$ where a represents the stretching constant. The physical flow model is sketched in Fig. 1. The regulatory expressions given the aforesaid postulates are declared below [16,25,38]:

Continuity equation:

$$\frac{\partial u}{\partial x} + \frac{\partial u}{\partial y} = 0 \tag{1}$$

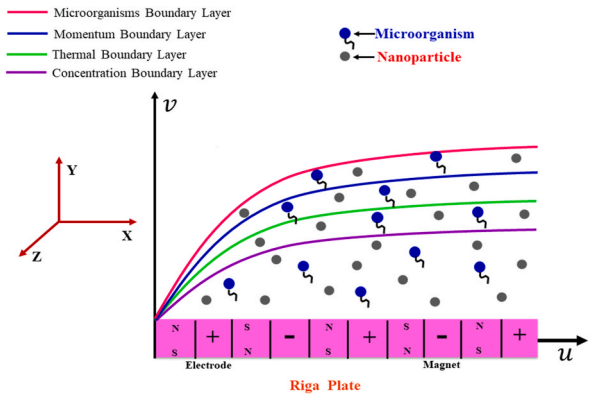

Fig. 1. Schematic representation of flow model.

Momentum equation:

$$\frac{\partial u}{\partial t}+u\frac{\partial u}{\partial x}+v\frac{\partial u}{\partial y}=\frac{\partial^2 u}{\partial y^2}\left[1+\lambda_1{}^2\left(\frac{\partial u}{\partial y}\right)^2\right]^{0.5(n-1)}\upsilon+\lambda_1{}^2\left[1+\lambda_1{}^2\left(\frac{\partial u}{\partial y}\right)^2\right]^{0.5(n-3)}\upsilon(n-1)\frac{\partial^2 u}{\partial y^2}\left(\frac{\partial u}{\partial y}\right)^2 +\frac{\pi J_0 M_0}{8\rho_f}\exp\left(-\frac{\pi}{a_1}y\right)-\frac{1}{\rho_f}(\rho_m-\rho_f)g\gamma(\overline{N}-\overline{N}_\infty)-(\rho_p-\rho_f)\frac{1}{\rho_f}g(C-C_\infty) +(1-C_\infty)g\Lambda_1(T-T_\infty) \tag{2}$$

Energy equation:

$$\frac{\partial T}{\partial t}+u\frac{\partial T}{\partial x}+v\frac{\partial T}{\partial y}+\frac{1}{\rho c_p}\frac{\partial q_r}{\partial y}=\nabla\left\{D_B\left(\frac{\partial T}{\partial y}\frac{\partial C}{\partial y}\right)+\frac{D_T}{T_\infty}\left(\frac{\partial T}{\partial y}\right)^2\right\}+\frac{\kappa}{\rho c_p}\frac{\partial^2 T}{\partial y^2} \tag{3}$$

Concentration equation:

$$\frac{\partial C}{\partial t}+u\frac{\partial C}{\partial x}+v\frac{\partial C}{\partial y}-\frac{D_T}{T_\infty}\frac{\partial^2 T}{\partial y^2}=D_B\frac{\partial^2 C}{\partial y^2}-k_r{}^2(C-C_\infty)\left(\frac{T}{T_\infty}\right)^l\exp\left(\frac{-E_a}{K_1 T}\right) \tag{4}$$

Motile bacteria's equation:

$$\frac{\partial \overline{N}}{\partial t}+u\frac{\partial \overline{N}}{\partial x}+v\frac{\partial \overline{N}}{\partial y}-D_n\frac{\partial^2 \overline{N}}{\partial y^2}=-\frac{b_c W_c}{(C_w-C_\infty)}\frac{\partial C}{\partial y}\frac{\partial \overline{N}}{\partial y}-\frac{b_c W_c \overline{N}}{(C_w-C_\infty)}\frac{\partial^2 C}{\partial y^2} \tag{5}$$

In this work, the fluid is considered optically dense. As a result, the Rosseland approximation is utilize to express radiative heat flux as [22]: $q_r = -\frac{4\sigma^*}{3k^*}\frac{\partial T^4}{\partial y}$, where σ^* and k^* stand for the Stefan-Boltzmann constant and the mean absorption coefficient respectively. Again, within the boundary layers of this bioconvective nanofluid model, the temperature difference is considered sufficiently trivial. By expanding T^4 in terms of T_∞ in the Taylor series and disregarding the higher order terms, the implicit differentiation of the radiative heat flux is gained as: $\frac{\partial q_r}{\partial y} = -\frac{16\sigma^* T_\infty^3}{3k^*}\frac{\partial^2 T}{\partial y^2}$. As a consequence, the modified energy equation with the help of Eq. (3) is rearranged by:

$$\frac{\partial T}{\partial t}+u\frac{\partial T}{\partial x}+v\frac{\partial T}{\partial y}=\frac{\kappa}{\rho c_p}\left[1+\frac{16\sigma^* T_\infty{}^3}{3k^*\kappa}\right]\frac{\partial^2 T}{\partial y^2}+\nabla\left\{D_B\left(\frac{\partial T}{\partial y}\frac{\partial C}{\partial y}\right)+\frac{D_T}{T_\infty}\left(\frac{\partial T}{\partial y}\right)^2\right\} \tag{6}$$

The stream characteristics at the sensor plate are specified as

$$u=U_0=ax; v=0; T=T_w; C=C_w=; \overline{N}=\overline{N}_w \text{ at } y=0\} \tag{7}$$

Furthermore, far away from the sensor plate, the flow attribute is stated as

$$u\to 0; T\to T_\infty; C\to C_\infty; \overline{N}\to\overline{N}_\infty \text{ as } y\to\infty\} \tag{8}$$

in Eqs. (1)–(8), (x, y) represent Cartesian coordinates, (u, v) denote velocity components, ρ_m microbe's density, ρ_p nanomaterials density, and ρ_f fluid density. To make a dimensionless form of the involved governing equations, the subsequent invariants are taken:

$$\left.\begin{aligned} &X=\frac{xU_0}{\upsilon}, Y=\frac{yU_0}{\upsilon}, U=\frac{u}{U_0}, V=\frac{v}{U_0}, \tau=\frac{tU_0{}^2}{\upsilon}, E_P=\frac{N_G T_\infty \upsilon^2}{\kappa(T_w-T_\infty)U_0{}^2}\\ &\theta=(T_w-T_\infty)^{-1}(T-T_\infty), N=(\overline{N}-\overline{N}_\infty)(\overline{N}_w-\overline{N}_\infty)^{-1}, \varphi=(C-C_\infty)(C_w-C_\infty)^{-1}\end{aligned}\right\} \tag{9}$$

By applying the proper non-dimensional quantities of Eq. (9) on the dimensional Eqs. (1)–(5), the respective equations are transformed into dimensionless which are expressed in Eqs. (10)–(14).

$$\frac{\partial U}{\partial X}+\frac{\partial V}{\partial Y}=0 \tag{10}$$

$$\frac{\partial U}{\partial \tau}=\frac{\partial^2 U}{\partial Y^2}\left[1+W_e\left(\frac{\partial U}{\partial Y}\right)^2\right]^{0.5(n-1)}+\frac{\partial^2 U}{\partial Y^2}\left(\frac{\partial U}{\partial Y}\right)^2 W_e(n-1)\left[1+W_e\left(\frac{\partial U}{\partial Y}\right)^2\right]^{0.5(n-3)} +Pe^{-SY}+\eta_m(\theta-N_r\varphi-R_b N)-U\frac{\partial U}{\partial X}-V\frac{\partial U}{\partial Y} \tag{11}$$

$$\frac{\partial \theta}{\partial \tau}=\frac{1}{P_r}\left(1+\frac{4}{3}R_n\right)\frac{\partial^2 \theta}{\partial Y^2}+N_t\left(\frac{\partial \theta}{\partial Y}\right)^2+N_b\left(\frac{\partial \theta}{\partial Y}\frac{\partial \varphi}{\partial Y}\right)-U\frac{\partial \theta}{\partial X}-V\frac{\partial \theta}{\partial Y} \tag{12}$$

$$\frac{\partial \varphi}{\partial \tau}=\frac{1}{S_c}\left(\frac{\partial^2 \varphi}{\partial Y^2}+\frac{N_t}{N_b}\frac{\partial^2 \theta}{\partial Y^2}\right)-K_c(1+l\delta_T\theta)(1-A_e+A_e\delta_T\theta)\varphi-U\frac{\partial \varphi}{\partial X}-V\frac{\partial \varphi}{\partial Y} \tag{13}$$

$$\frac{\partial N}{\partial \tau}=\frac{1}{L_b}\frac{\partial^2 N}{\partial Y^2}-\frac{P_e}{L_b}\left[\frac{\partial \varphi}{\partial Y}\frac{\partial N}{\partial Y}+(\Omega+N)\frac{\partial^2 \varphi}{\partial Y^2}\right]-U\frac{\partial N}{\partial X}-V\frac{\partial N}{\partial Y} \tag{14}$$

The involved parameters that have a strong effect on the current designed Carreau nanofluid flow model are acknowledged as Weissenberg number (W_e): $\frac{\lambda_1^2 U_0^4}{\upsilon}$, mixed convection factor (η_m): $\frac{\upsilon g\Lambda_1(1-C_\infty)(T_w-T_\infty)}{U_0^3}$, buoyancy ratio parameter (N_r): $\frac{(\rho_p-\rho_f)(C_w-C_\infty)}{\Lambda_1\rho_f(1-C_\infty)(T_w-T_\infty)}$, bioconvection-Rayleigh number (R_b): $\frac{\gamma(\rho_m-\rho_f)(\overline{N}_w-\overline{N}_\infty)}{\Lambda_1\rho_f(1-C_\infty)(T_w-T_\infty)}$, modified Hartmann number (P): $\frac{\pi J_0 M_0 \nu}{8\rho_f U_0^3}$, the width of magnets and electrode (S): $\frac{\pi\nu}{\alpha_1 U_0}$, Prandtl number ($P_r$): $\frac{\rho c_p \upsilon}{\kappa}$, radiation parameter ($R_n$): $\frac{4\sigma^* T_\infty^3}{\kappa k^*}$, thermophoresis parameter (N_t): $\frac{\Delta D_T(T_w-T_\infty)}{T_\infty \upsilon}$, Brownian motion parameter (N_b): $\frac{\Delta D_B(C_\infty-C_\infty)}{\upsilon}$, Schmidt number ($S_c$): $\frac{\upsilon}{D_B}$, chemical reaction parameter (K_c): $\frac{\upsilon k_r^2}{U_0^2}$, temperature difference parameter (α_1): $\frac{(T_w-T_\infty)}{T_\infty}$, activation energy parameter (A_e): $\frac{E_a}{k_1 T_\infty}$, bio-convection Lewis number (L_b): $\frac{\upsilon}{D_n}$, bio-Peclet number (P_e): $\frac{b_c w_c}{D_n}$, and bio-convection concentration difference parameter (α_3): $\frac{\overline{N}_\infty}{\overline{N}_w-\overline{N}_\infty}$. Additionally, stream function ψ correlates with velocity constituents as like $V=-\frac{\partial \psi}{\partial U}$ and $U=\frac{\partial \psi}{\partial Y}$, that satisfies the continuity Eq. (10). Furthermore, the changed situations of the sensor surface and away from the sensor surface are explained in Eq. (15).

$$\left.\begin{array}{l} U=0, V=0, \theta=1, \varphi=1, N=1 \ \text{ at } \ Y=0 \\ U\to 0, \theta\to 0, \varphi\to 0, N\to 0 \ \ as \ Y\to\infty \end{array}\right\} \tag{15}$$

Because of engineering and scientific perspectives, the physical parameters of interest including heat transport, have productive applicability. Further, the dimensionless shape of significant engineering quantities such as Nusselt number (Nu) [41] and skin friction (Cf) [16] for the Carreau nano-bioconvective system are precisely configured as like Eq. (16).

$$\left.\begin{array}{l} \mathrm{Nu}=\left[-\left(1+\frac{4}{3}R_n\right)\frac{\partial \theta}{\partial Y}\right]_{Y=0}, \mathrm{Cf}=\left[\frac{\partial U}{\partial Y}\left\{1+W_e\left(\frac{\partial U}{\partial Y}\right)^2\right\}^{0.5(n-1)}\right]_{Y=0} \end{array}\right\} \tag{16}$$

3. Entropy production

The molecular disorder of the current designed structure can be measured through entropy production. Entropy production for Carreau nanofluid in the occurrence of swimming organisms and radiation can be communicated as [48,49]:

$$\begin{aligned} N_G=&\frac{\kappa}{{T_\infty}^2}\left(1+\frac{16\sigma^* {T_\infty}^3}{3\kappa K^*}\right)\left(\frac{\partial T}{\partial y}\right)^2+\frac{\mu}{T_\infty}\left[1+{\lambda_1}^2\left(\frac{\partial u}{\partial y}\right)^2\right]^{0.5(n-1)}\left(\frac{\partial u}{\partial y}\right)^2+\frac{LD_B}{T_\infty}\left(\frac{\partial T}{\partial y}\frac{\partial C}{\partial y}\right)\\ &+\frac{LD_B}{C_\infty}\left(\frac{\partial C}{\partial y}\right)^2+\frac{LD_B}{T_\infty}\left(\frac{\partial T}{\partial y}\frac{\partial N}{\partial y}\right)+\frac{LD_B}{N_\infty}\left(\frac{\partial N}{\partial y}\right)^2 \end{aligned} \tag{17}$$

On the right side of aforesaid Eq. (17), the initial term portrays the heat transport irreversibility, the succeeding term describes the fluid friction irreversibility, the third and four terms illustrate mass diffusion irreversibility, and the last two terms represent diffusion irreversibility due to swimming microbes. Given dimensionless variables referred to in Eq. (9), the reduced form of the entropy equation is delivered as [50]:

$$\begin{aligned} E_P=&\alpha_1\left(1+\frac{4}{3}R_n\right)\left(\frac{\partial \theta}{\partial Y}\right)^2+B_r\left(\frac{\partial U}{\partial Y}\right)^2\left[1+W_e\left(\frac{\partial U}{\partial Y}\right)^2\right]^{0.5(n-1)}+\alpha_2 R_1\frac{\partial \theta}{\partial Y}\frac{\partial \varphi}{\partial Y}\\ &+{\alpha_1}^{-1}{\alpha_2}^2 R_1\left(\frac{\partial \varphi}{\partial Y}\right)^2+\alpha_3 R_2\frac{\partial \theta}{\partial Y}\frac{\partial N}{\partial Y}+{\alpha_1}^{-1}{\alpha_3}^2 R_2\left(\frac{\partial N}{\partial Y}\right)^2 \end{aligned} \tag{18}$$

in the aforementioned Eq. (18), R_1 and R_2 depict the diffusion variable due to concentration and microbes.

4. Solution methodology

The regulatory system of Eqs. (10)–(14) portrays extremely non-linearity which it's tough to solve analytically. Therefore, the finite difference approach, a recognized numerical methodology is performed numerically to handle the regulatory problem.

4.1. Finite difference approach

In this segment, the solution's methodology, to resolve the underlying Eqs. (10)–(14) with the boundary conditions, is described by utilizing the well-known explicit finite difference method (EFDM). To use this finite difference method, the domain exclusive to the borderline is scattered into grid spaces by straight lines whose axes, X and Y, are parallel, where the X-axis is concentrated to the sensor plate, and the Y-axis is occupied to the upright direction on the sensor plate.

For solving this bioconvective Carreau nanofluid model, the subsequent assumptions, Eq. (17), are considered: altitude of the sheet: $X=20$, entire number of grids ahead X-axis: $M=100$, grid-space ahead X-direction: $\Delta X=0.20$; breadth of the sheet: $Y=50$; entire

number of grids ahead Y-direction: $N = 400$; grid-space ahead Y-direction: $\Delta Y = 0.125$, and time step: $\Delta\tau = 0.0001$. With the help of EFDM, the partial differentials can be expressed as Eq. (19).

$$\left.\begin{aligned}
&\frac{\partial U}{\partial X}=\frac{U_{i,j}-U_{i-1,j}}{\Delta X},\frac{\partial V}{\partial Y}=\frac{V_{i,j+1}-V_{i,j}}{\Delta Y},\frac{\partial U}{\partial \tau}=\frac{U^{'}_{i,j}-U_{i,j}}{\Delta \tau},\frac{\partial^2 U}{\partial Y^2}=\frac{U_{i,j+1}-2U_{i,j}+U_{i,j-1}}{(\Delta Y)^2},\\
&\frac{\partial U}{\partial Y}=\frac{U_{i,j+1}-U_{i,j}}{\Delta Y},\frac{\partial \theta}{\partial \tau}=\frac{\theta^{'}_{i,j}-\theta_{i,j}}{\Delta \tau},\frac{\partial \theta}{\partial X}=\frac{\theta_{i,j}-\theta_{i-1,j}}{\Delta X},\frac{\partial \theta}{\partial Y}=\frac{\theta_{i,j+1}-\theta_{i,j}}{\Delta Y},\frac{\partial^2 \theta}{\partial Y^2}=\frac{\theta_{i,j+1}-2\theta_{i,j}+\theta_{i,j-1}}{(\Delta Y)^2},\\
&\frac{\partial \varphi}{\partial \tau}=\frac{\varphi^{'}_{i,j}-\varphi_{i,j}}{\Delta \tau},\frac{\partial \varphi}{\partial X}=\frac{\varphi_{i,j}-\varphi_{i-1,j}}{\Delta X},\frac{\partial \varphi}{\partial Y}=\frac{\varphi_{i,j+1}-\varphi_{i,j}}{\Delta Y},\frac{\partial^2 \varphi}{\partial Y^2}=\frac{\varphi_{i,j+1}-2\varphi_{i,j}+\varphi_{i,j-1}}{(\Delta Y)^2},\frac{\partial N}{\partial \tau}=-\frac{N^{'}_{i,j}-N_{i,j}}{\Delta \tau},\\
&\frac{\partial N}{\partial X}=\frac{N_{i,j}-N_{i-1,j}}{\Delta X},\frac{\partial N}{\partial Y}=\frac{N_{i,j+1}-N_{i,j}}{\Delta Y},\frac{\partial^2 N}{\partial Y^2}=\frac{N_{i,j+1}-2N_{i,j}+N_{i,j-1}}{(\Delta Y)^2}
\end{aligned}\right\} \tag{19}$$

So, after implementing this finite difference tool, the constructed dimensionless regulatory Eqs. (10)–(14) can be represented in the following patterns:

$$V_{i,j}=V_{i,j-1}-\left[\left(U_{i,j}-U_{i-1,j}\right)\frac{\Delta Y}{\Delta X}\right] \tag{20}$$

$$U^{'}_{i,j}=U_{i,j}+\Delta\tau\left[\begin{aligned}
&\left(\frac{U_{i,j+1}-2U_{i,j}+U_{i,j-1}}{(\Delta Y)^2}\right)\left\{1+W_e\left(\frac{U_{i,j+1}-U_{i,j}}{\Delta Y}\right)^2\right\}^{0.5(n-1)}-U_{i,j}\left(\frac{U_{i,j}-U_{i-1,j}}{\Delta X}\right)\\
&+W_e(n-1)\left(\frac{U_{i,j+1}-U_{i,j}}{\Delta Y}\right)^2\left(\frac{U_{i,j+1}-2U_{i,j}+U_{i,j-1}}{(\Delta Y)^2}\right)\left\{1+W_e\left(\frac{U_{i,j+1}-U_{i,j}}{\Delta Y}\right)^2\right\}^{0.5(n-3)}\\
&+Pe^{-SY}+\eta_m\left(\theta_{i,j}-N_r\varphi_{i,j}-R_bN_{i,j}\right)-V_{i,j}\left(\frac{U_{i,j+1}-U_{i,j}}{\Delta Y}\right)
\end{aligned}\right] \tag{21}$$

$$\theta^{'}_{i,j}=\theta_{i,j}+\Delta\tau\left[\begin{aligned}
&\frac{1}{P_r}\left(1+\frac{4}{3}R_n\right)\left(\frac{\theta_{i,j+1}-2\theta_{i,j}+\theta_{i,j-1}}{(\Delta Y)^2}\right)-U_{i,j}\left(\frac{\theta_{i,j}-\theta_{i-1,j}}{\Delta X}\right)-V_{i,j}\left(\frac{\theta_{i,j+1}-\theta_{i,j}}{\Delta Y}\right)\\
&+N_t\left(\frac{\theta_{i,j+1}-\theta_{i,j}}{\Delta Y}\right)^2+N_b\left(\frac{\theta_{i,j+1}-\theta_{i,j}}{\Delta Y}\right)\left(\frac{\varphi_{i,j+1}-\varphi_{i,j}}{\Delta Y}\right)
\end{aligned}\right] \tag{22}$$

$$\varphi^{'}_{i,j}=\varphi_{i,j}+\Delta\tau\left[\begin{aligned}
&\frac{1}{S_c}\left(\frac{\varphi_{i,j+1}-2\varphi_{i,j}+\varphi_{i,j-1}}{(\Delta Y)^2}\right)-U_{i,j}\left(\frac{\varphi_{i,j}-\varphi_{i-1,j}}{\Delta X}\right)-V_{i,j}\left(\frac{\varphi_{i,j+1}-\varphi_{i,j}}{\Delta Y}\right)\\
&+\frac{1}{S_c}\left(\frac{\theta_{i,j+1}-2\theta_{i,j}+\theta_{i,j-1}}{(\Delta Y)^2}\right)\left(\frac{N_t}{N_b}\right)-K_c\left(1+l\delta_T\theta_{i,j}\right)\varphi_{i,j}\left(1-A_e+A_e\delta_T\theta_{i,j}\right)
\end{aligned}\right] \tag{23}$$

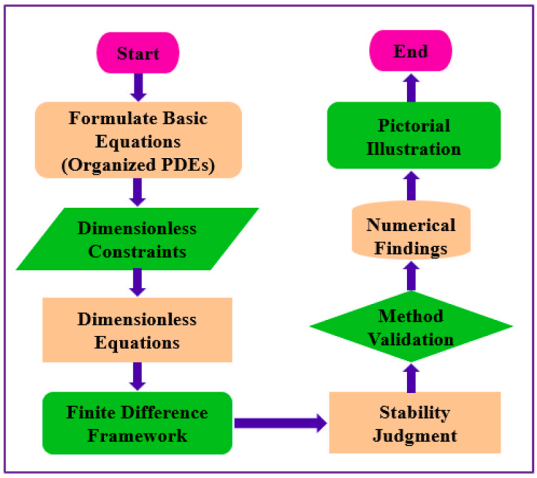

Fig. 2. A general framework for this numerical analysis.

$$N_{i,j}^{'} = N_{i,j} + \Delta\tau \left[\begin{array}{l} \frac{1}{L_b}\left(\frac{N_{i,j+1} - 2N_{i,j} + N_{i,j-1}}{(\Delta Y)^2}\right) - U_{i,j}\left(\frac{N_{i,j} - N_{i-1,j}}{\Delta X}\right) - V_{i,j}\left(\frac{N_{i,j+1} - N_{i,j}}{\Delta Y}\right) \\ -\frac{P_e}{L_b}(\Omega + N)\left(\frac{\varphi_{i,j+1} - 2\varphi_{i,j} + \varphi_{i,j-1}}{(\Delta Y)^2}\right) - \frac{P_e}{L_b}\left(\frac{\varphi_{i,j+1} - \varphi_{i,j}}{\Delta Y}\right)\left(\frac{N_{i,j+1} - N_{i,j}}{\Delta Y}\right) \end{array} \right] \tag{24}$$

From Eqs. (21)–(24), the value of fluid velocity, temperature, concentration, and density of microorganism profiles are received respectively. The associated boundary constraints are:

$$\left.\begin{array}{l} U_{i,0}^{\hbar} = 1, V_{i,0}^{\hbar} = 0, \theta_{i,0}^{\hbar} = 1, \varphi_{i,0}^{\hbar} = 1, N_{i,0}^{\hbar} = 1 \Big\} \text{ at } Y = 0 \\ U_{i,\Pi}^{\hbar} = 0, \theta_{i,\Pi}^{\hbar} \to 0, \varphi_{i,\Pi}^{\hbar} \to 0, N_{i,\Pi}^{\hbar} \to 0 \Big\} \text{ as } Y \to \infty, \text{where } \Pi \to \infty \end{array}\right\} \tag{25}$$

Here, grid points with X and Y coordinates are characterized by the subscripts i and j, and the superscript $\hbar$ indicates the time value, $\tau = \hbar\Delta\tau$ (where $\hbar = 1, 2, 3 \ldots$). The above-mentioned governing Eqs. (20)–(25) offer the numerical results using this bioconvective Carreau nanofluid flow problem. Conclusively, a general framework is depicted in Fig. 2 to understand the whole numerical process of the current study.

4.2. Stability analysis

Here, an effective explicit FDM is applied for handling the regulatory equations. Mentioned that explicit technique is conditionally stable. So, the analysis of stability is extremely essential for picking the appropriate values of involved factors for the current designed bioconvective Carreau nanofluid flow model.

By using suitable operations on Eqs. (21)–(24), the stability restrictions have been offered as:

$$U\frac{\Delta\tau}{\Delta X} + |-V|\frac{\Delta\tau}{\Delta Y} + \frac{1}{P_r}\left(1 + \frac{4}{3}R_n\right)\frac{2\Delta\tau}{(\Delta Y)^2} - N_b\frac{2\Delta\tau}{(\Delta Y)^2}\varphi - N_t\frac{2\Delta\tau}{(\Delta Y)^2}\theta \le 1 \tag{26}$$

$$U\frac{\Delta\tau}{\Delta X} + |-V|\frac{\Delta\tau}{\Delta Y} + \frac{1}{S_c}\frac{2\Delta\tau}{(\Delta Y)^2} + \frac{\Delta\tau K_c}{2}(1 + l\delta\theta)(1 - \mathrm{A}_e + \mathrm{A}_e\delta\theta) \le 1 \tag{27}$$

$$U\frac{\Delta\tau}{\Delta X} + |-V|\frac{\Delta\tau}{\Delta Y} + \frac{1}{L_b}\frac{2\Delta\tau}{(\Delta Y)^2} + \left(\frac{P_e}{L_b}\right)\frac{2\Delta\tau}{(\Delta Y)^2}\varphi \le 1 \tag{28}$$

in this assessment, $N = 0$, $\theta = 0$, $V = 0$, $U = 0$, $\varphi = 0$ at $\tau = 0$ are the initial situations of the current flow model. For $\Delta\tau = 0.0001$, $\Delta X = 0.2$, and $\Delta Y = 0.125$, the convergence conditions of the present paradigm, by using Eqs. (26)–(28), are calculated as $P_r \ge 0.0213$, $S_c \ge 0.0128$, and $L_b \ge 0.0128$.

5. Outcomes confirmation

This segment affirms the accuracy of computed current outcomes. Table 1 is designed as an appraisal of existing outputs for skin friction with Hayat et al. [14] and Parvez et al. [19]. This tabular outcome shows a worthy settlement of the present result with prior outputs.

Also, the heat transportation results are documented in Table 2 with prior outcomes of Khan and Pop [3], Khan et al. [4], and Rana et al. [30]. This tabular finding settled that ongoing results are in decent settlement with the disclosed results.

6. Results and discussion

This portion is designed to discuss the physical insight of effective factors on the Carreau nanomaterial flow problem produced from the Riga plate with the swimming of microbes. The numerical outcomes are calculated via CVF6.6a. Physical depiction of crucial

Table 1
Computational outputs of skin friction when n = 3.0.

W_e	Hayat et al. [14]	Parvez et al. [19]	Current observation
0.0	1.0000	1.0005	1.0005
0.1	1.0158	1.0163	1.0162
0.2	1.0347	1.0359	1.0358
0.3	1.0548	1.0562	1.0560
0.4	1.0755	1.0767	1.0767
0.5	1.0962	1.0974	1.0972

Table 2
Outputs comparison of the thermal transmission.

N_b=N_t	Khan and Pop [3]	Khan et al. [4]	Rana et al. [30]	Current outcomes
0.10	0.9524	0.9541	0.95410	0.95410
0.20	0.3654	0.3667	0.36670	0.36670
0.30	0.1355	0.1359	0.13591	0.13591
0.40	0.0495	0.0499	0.04990	0.04990
0.50	0.0179	0.0185	0.01852	0.01852

variables like W_e, P, N_r, R_b, N_b, N_t, K_c, A_e, S_c, B_r, and L_b are reported.

6.1. Analyses of fluid motion

The physical behavior of bio-Rayleigh number (R_b), modified Hartmann number (P), Weissenberg number (W_e), and buoyancy relative variable (N_r) on fluid velocity distribution (U) are depicted in Fig. (3)-(6). In Fig. 3 the modification on fluid motion for R_b is visualized. The greater values of R_b generate the opposing buoyancy forces that restrict the fluid velocity. So, the fluid velocity is downward due to an upsurge of R_b. On the other hand, the velocity field and boundary layer thickness became upward for rising values of P that are portrayed in Fig. 4. Generally, the velocity modification is a reducing function of the Hartman number. But, in this instance, the Lorentz force which is produced by the alternating of a variety of magnets and electrodes of the Riga plate upsurges the motion of fluid.

Moreover, the control of W_e on fluid velocity is described in Fig. 5 where the material variable (W_e) has a positive influence on the motion of nanofluid. Furthermore, the varying values of N_r, in Fig. 6, cause a lessening in velocity distribution. Physically, N_r opposes buoyancy force that augments the conflict to moving fluid particles. As a consequence, N_r makes a negative effect on the velocity arrangement (U) of nanomaterial.

6.2. Analyses of thermal energy

The physical description of the thermo-migration factor (N_t), random movement variable (N_b), and radiation factor (R_n) on nanofluid thermal distribution (θ) are plotted in Figs. (7)-(9). Fig. 7 exhibits the effect of N_b in the temperature profile (θ). With the enhancement of the value of N_b, the random movement of nanoparticles is going to upsurge. As a result, the thermal field of the nanofluid is improved. Also, Fig. 8 demonstrates the consequence of N_t in the temperature profile. Due to the increase of N_t, a thermophoretic force occurs which migrates the nanoparticle from a higher temperature to a lower.

As a consequence, nanomaterial's thermal distribution is enhanced via greater N_t. Further, the radiation R_n impact on thermal distribution is articulated in Fig. 9. Additional value of R_n offers additional heat to the working fluid which strengthens the thermal distribution of nanofluid.

6.3. Analyses of concentration

The effect of Arrhenius activation energy (A_e), Schmidt number (S_c), and chemical reaction factor (K_c) on fluid concentration field

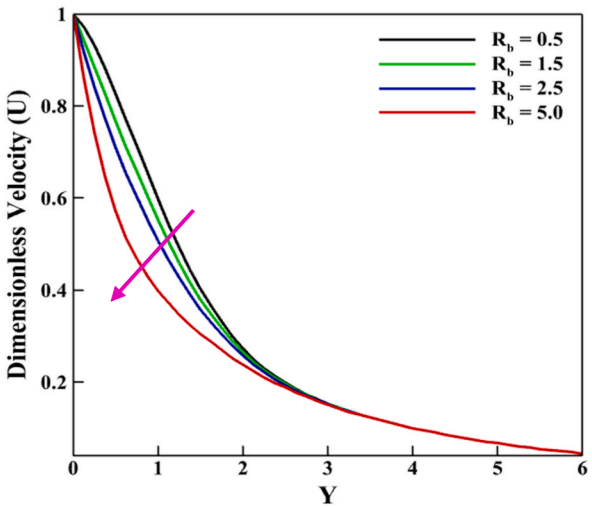

Fig. 3. Depiction of U for R_b.

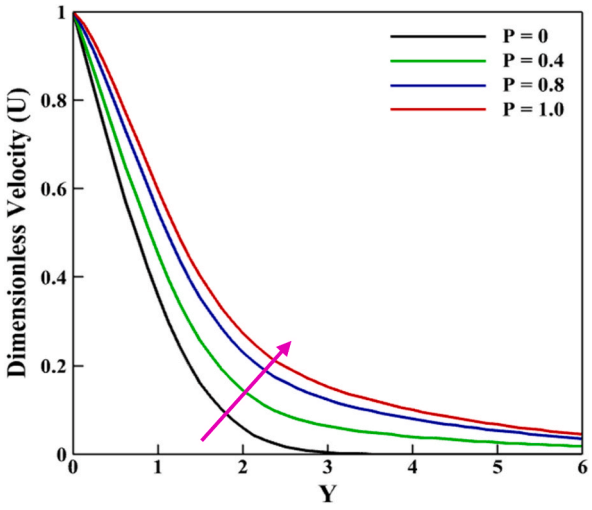

Fig. 4. Depiction of U for P.

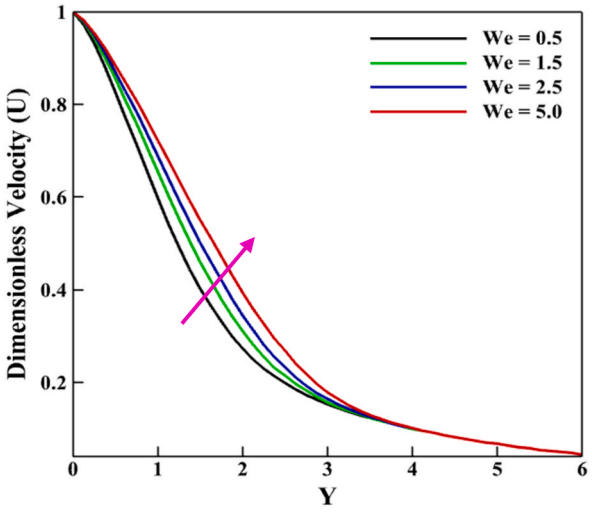

Fig. 5. Depiction of U for W_e.

(φ) are graphically and physically explained in Figs. (10)-(12). Here, Fig. 10 depicts the behavior of A_e on nanomaterial concentration distribution. It is clear that without Arrhenius activation energy ($A_e = 0$), the concentration profile is lower than the others. Physically, the higher values of A_e endorse the chemical reaction of the nanofluid that boosts the concentration distribution of nanomaterial. Fig. 11 exhibits the effect of S_c in the concentration field profile. The larger S_c decays molecular diffusivity which consequently diminishes nanomaterial concentration distribution. Furthermore, the consequence of K_c is displayed in Fig. 12. Due to the increment of K_c, the concentration profile is declined. K_c significantly improves the dissipation of fluid movement that decays the fluid concentration.

6.4. Analyses of motile bacteria

The distribution of motile microbes (N) as bio-Lewis number (L_b) and Peclet number (P_e) raises is described in Figs. 13 and 14. For the greater estimation of L_b, the lower diffusivity of microorganisms occurred which reduced the distribution of motile bacteria (see Fig. 13). The influence of P_e that has contributed to the swimming of microbes is described in Fig. 14. The higher values of P_e lead to less diffuse of motile bacteria which decays the distribution of motile microbes for the whole fluid domain. The role of activation energy (A_e) on motile microbes (N) is highlighted in Fig. 15. Higher (A_e) strengthens the density of concentration which intensifies the distribution of motile microbes.

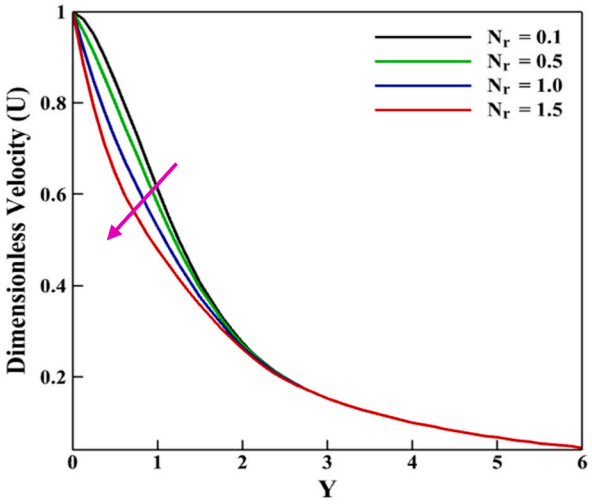

Fig. 6. Depiction of U for N_r.

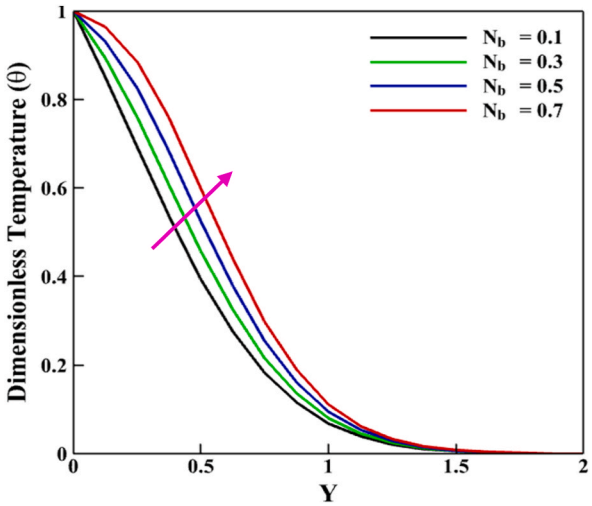

Fig. 7. Depiction of θ for N_b.

6.5. *Analyses of 3D surface and contour plot*

In Fig. 16(a–f), the interactive effects of crucial parameters like thermo-migration parameter (N_t), random motion variable (N_b), and radiation factor (R_n) for heat transfer rate (Nu) in the current design system are described via surface and contour plots. The modification in heat deliveries of the nanofluidic system is reduced via a greater approximation of N_t and N_b, but the opposite behavior exists for R_n. Moreover, the entropy production (E_p) in the nanofluidic scheme using Eq. (18) for pivotal variables like Brinkman number (B_r), radiation variable (R_n), and Weissenberg variable (W_e) is also described in Fig. 17(a–f), where this figure is designed to show the variations of E_p through the 3D surface and 2D contour plots. The B_r heightens the internal friction of fluid molecules which boosts E_p. Also, the Weissenberg variable and the radiation factor widen the entropy production in the current designed system. Physically, greater R_n widens radiation emission which heightens collision among fluid particles. Thus, the production of entropy is amplified.

7. Conclusions

In this in-depth research, characteristics of chemically reactive nanomaterial for bio-convective flow along Riga's stretchy surface with swimming bacteria are discussed. Arrhenius type of reacting species is addressed to describe the mass transportation operation. An efficient computational approach, finite difference is used to tackle the regulatory problem. Entropy production is measured. The key findings are noted below:

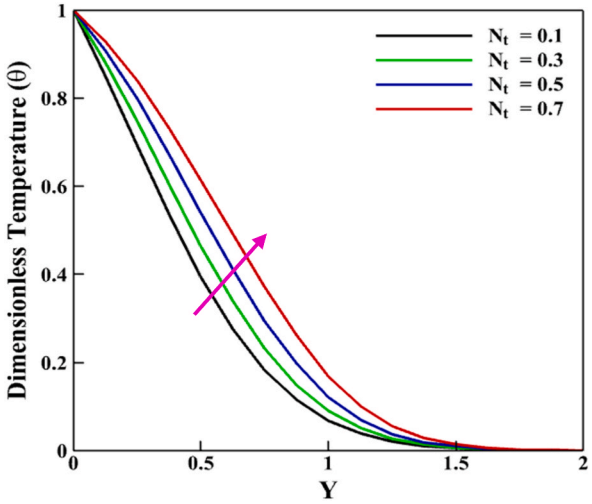

Fig. 8. Depiction of θ for N_t.

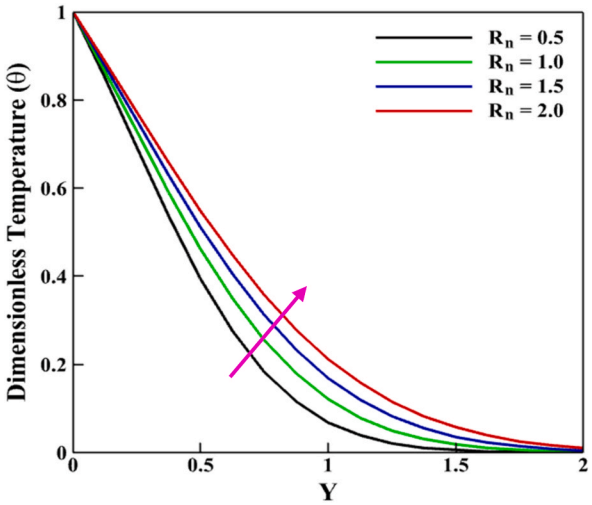

Fig. 9. Depiction of θ for R_n.

- Radiation parameter strengthens the temperature of nanofluid whereas heat transportation rate and entropy production exhibit similar outcomes for radiation factor.
- The entropy production is enhanced by the Weissenberg variable and Brinkman parameter.
- Modified Hartmann number intensifies the potency of the electric field which heightens the motion of fluid.
- Activation energy variables and chemical reaction parameter exhibit opposite impacts on the concentration of nanomaterial.
- The developing values of bio-Lewis number produced a drop in the diffusion of microbes and it makes hindrance in the movement of microbes.
- Heat transportation of nanomaterial decays via Random motion and thermo-migration parameters.

This analysis portrays an effective role in cooling systems, thermal management systems, drug transportation, cancer treatment, biofuels, and mining industries. This research effort can be extended by incorporating multiple flow behaviors such as ternary nanoparticles, exponential heat source, quadratic radiation, and mass transpiration. Some other nanofluidic models such as Williamson, Casson, Prandtl-Erying, and Carreau-Yasuda may be used to see more rheological effects on Riga sheet with microbes and Arrhenius catalysts.

Data availability statement

Data will be made available on request.

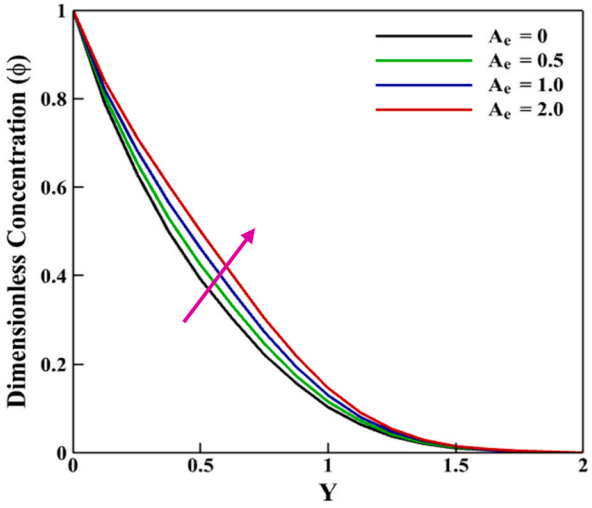

Fig. 10. Depiction of φ for A_e.

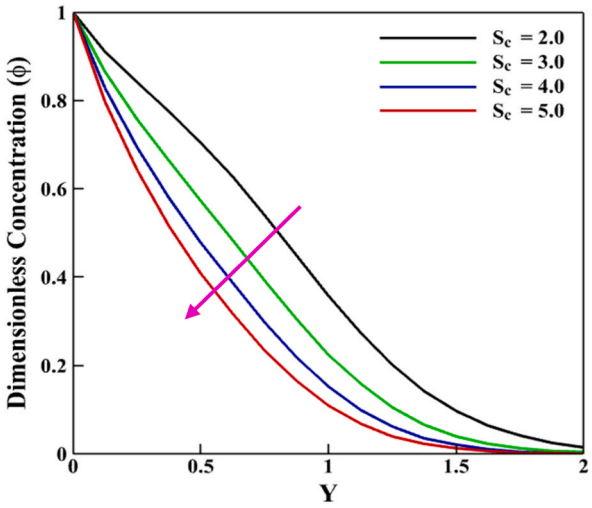

Fig. 11. Depiction of φ for S_c.

CRediT authorship contribution statement

Saiful Islam: Investigation, Writing – original draft, Formal analysis. **B.M.J. Rana:** Formal analysis, Writing – original draft. **Md Shohel Parvez:** Formal analysis, Writing – original draft. **Md Shahadat Hossain:** Formal analysis, Investigation. **Malati Mazumder:** Investigation, Writing – review & editing. **Kanak Chandra Roy:** Formal analysis, Writing – review & editing. **M.M. Rahman:** Conceptualization, Supervision.

Declaration of competing interest

The authors declare that they have no known competing financial interests or personal relationships that could have appeared to influence the work reported in this paper.

Nomenclature

A_e	Activation energy factor [−]
a_1	Absorption coefficient [m^{-1}]
B_r	Brinkman variable [−]
C	Concentration of fluid [mol m^{-3}]

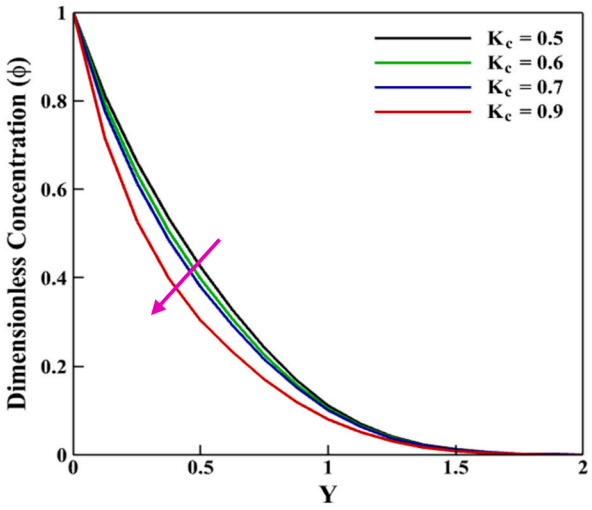

Fig. 12. Depiction of φ for K_c.

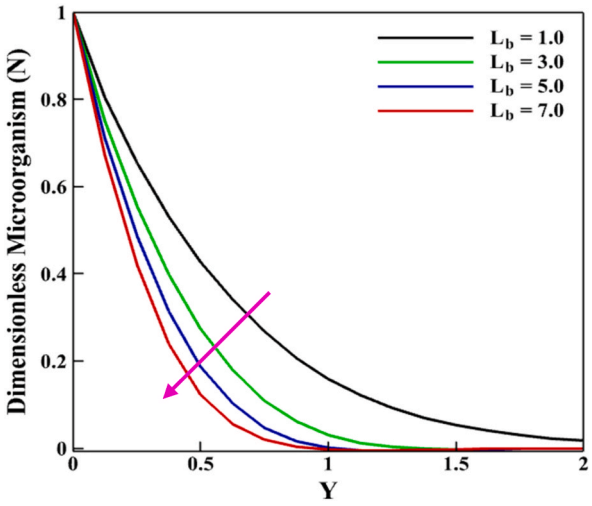

Fig. 13. Depiction of N for L_b.

Cf	Dimensionless skin friction [−]
Cp	Specific heat capacitance [J kg^{-1} K^{-1}]
Cw	Fluid concentration at the sheet [mol m^{-3}]
C_∞	Ambient concentration [mol m^{-3}]
D_B	Brownian diffusion, [m^2 s^{-1}]
Dn	Microbes' diffusion [m^2 s^{-1}]
D_T	Heat diffusion [m^2 s^{-1}]
E_o	Electric field intensity [m kg s^{-3} A^{-1}]
J_0	Density of current [Am^{-2}]
K_c	Chemical reaction parameter [−]
L	Ideal gas constant [−]
L_b	Bioconvection Lewis number [−]
l	Unit fitted constant [−]
M_0	Magnetization of permanent magnets [$kgA^{-1}s^{-2}$]
N_b	Random motion variable [−]
N_d	Density number of microorganisms [−]
N_r	Buoyancy relative factor [−]
N_t	Thermo-migration factor [−]

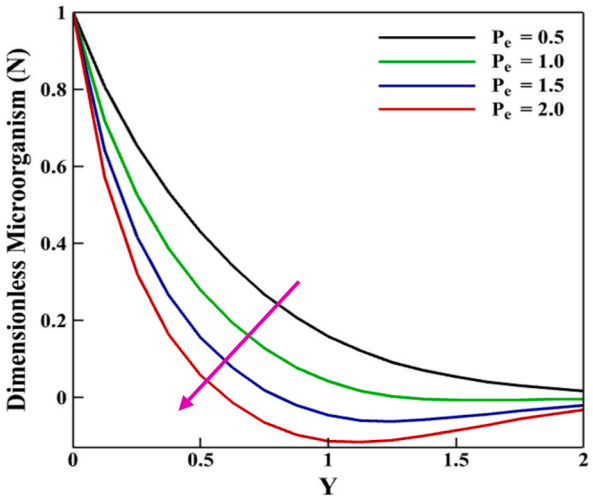

Fig. 14. Depiction of N for P_e.

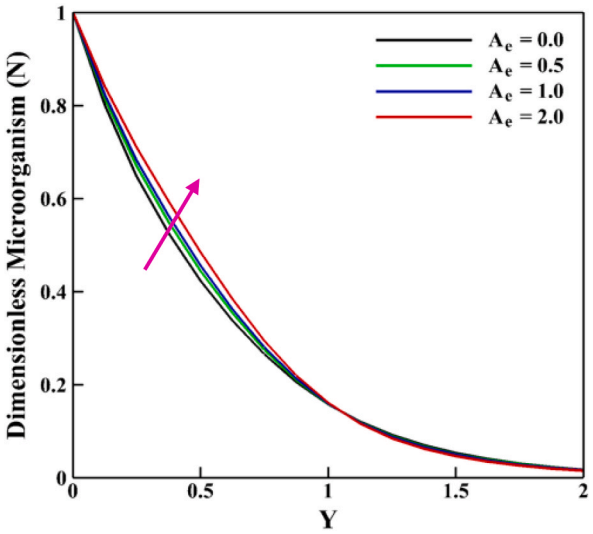

Fig. 15. Depiction of N for A_e.

P	Modified Hartmann number [−]
Pr	Prandtl variable [−]
Pe	Bio-Peclet number [−]
q_r	Radiative heat flux [kgm^{-2}]
R_b	Bio-Rayleigh variable [−]
R_n	Radiation parameter [−]
Nu	S Heat transportation [−] Breadth of the electrodes and magnets [m]
Sh	Mass transportation [−]
T	Temperature [K]
Tw	Temperature at surface [K]
$T\infty$	Temperature outside surface [K]
t	Time [s]
$\overline{N}$	Microorganisms [ms^{-1}]
N	Non-dimensional microorganisms [−]
W_c	Speed of microbes [m s^{-1}]

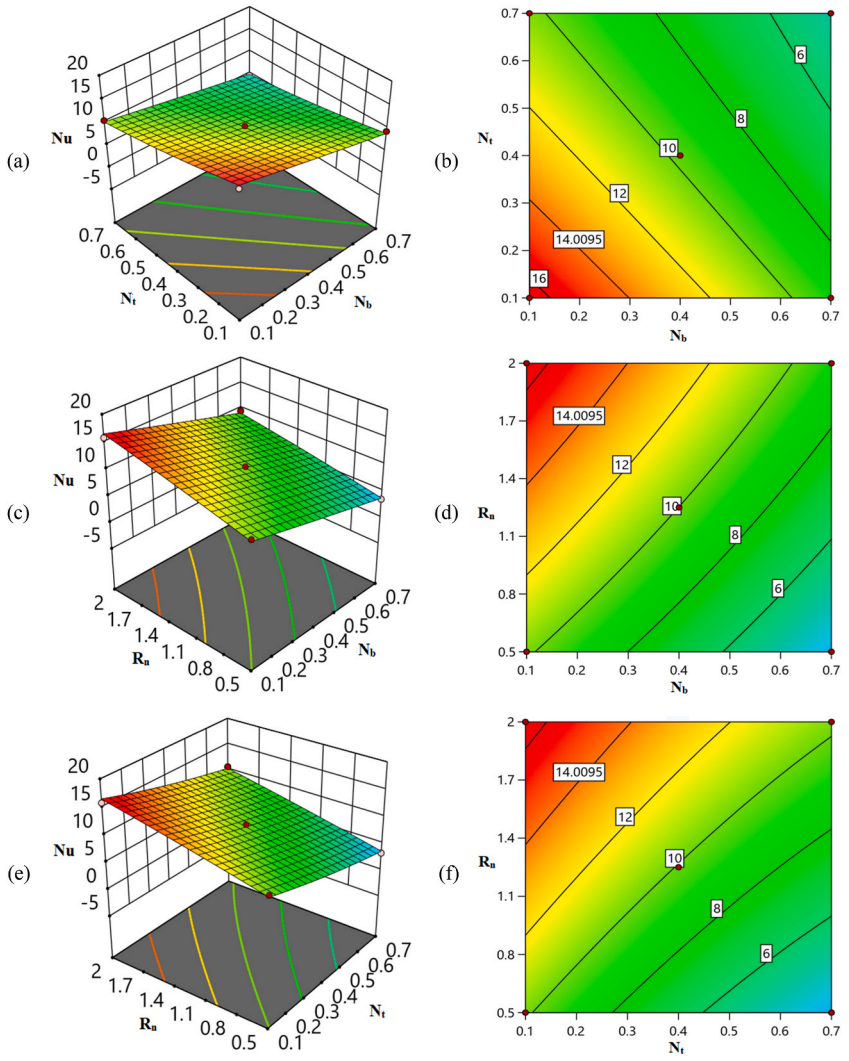

Fig. 16. 3D surface and contour plots for heat transportation.

Greek notations

η_m	Mixed convection parameter [−]
λ_1	Time material coefficient [−]
γ	Average volume of microbes [−]
σ	Electrical conductivity [s m^{-1}]
σ^*	Stefan-Boltzmann constant [W $m^{-2}K^{-4}$]
θ	Dimension-free temperature [−]
τ	Dimension-free time [−]
κ	Heat conductivity [W m^{-1} K^{-1}]
κ^*	Mean absorption coefficient [m^{-1}]
g	Gravitational acceleration [m s^{-2}]
Λ_1	Thermal expansion coefficient [K^{-1}]
ρ_f	Liquid density [kg m^{-3}]
ρ_m	Microbes' density [kg m^{-3}]
ρ_p	Nano-particles density [kg m^{-3}]
υ	Kinematic viscosity [m^2 s^{-1}]
φ	Dimensionless concentration [−]

Abbreviations

AL MHD Artificial Intelligence Magnetohydrodynamic

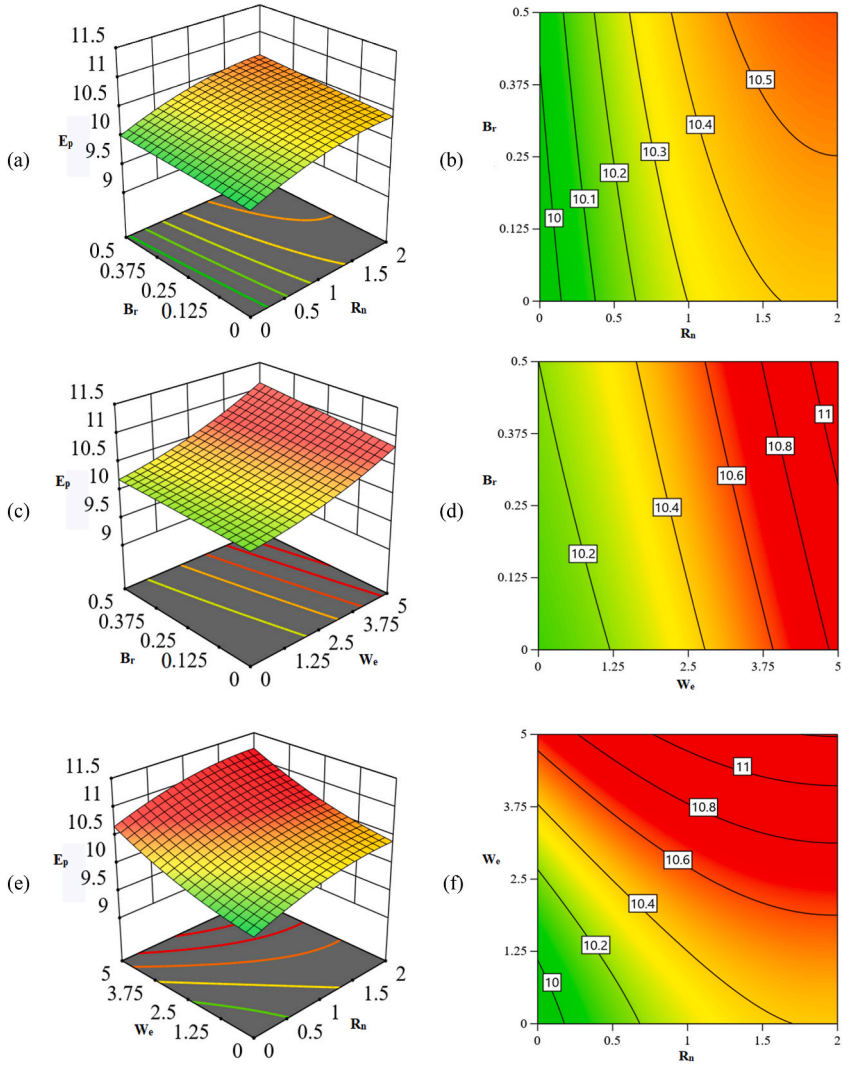

Fig. 17. 3D surface and contour plots for entropy production.

EMHD Electro-Magnetohydrodynamic

References

[1] S.U. Choi, J.A. Eastman, Enhancing Thermal Conductivity of Fluids with Nanoparticles (No. ANL/MSD/CP-84938, Argonne National Lab. (ANL), Argonne, IL (United States), 1995. CONF-951135-29).
[2] J. Buongiorno, Convective transport in nanofluids, J. Heat Tran. 128 (2006) 240–250.
[3] W.A. Khan, I. Pop, Boundary-layer flow of a nanofluid past a stretching sheet, Int. J. Heat Mass Tran. 53 (2010) 2477–2483.
[4] M.S. Khan, I. Karim, L.E. Ali, A. Islam, Unsteady MHD free convection boundary-layer flow of a nanofluid along a stretching sheet with thermal radiation and viscous dissipation effects, Int. Nano Lett. 2 (2012) 1–9.
[5] O.D. Makinde, W.A. Khan, Z.H. Khan, Buoyancy effects on MHD stagnation point flow and heat transfer of a nanofluid past a convectively heated stretching/shrinking sheet, Int. J. Heat Mass Tran. 62 (2013) 526–533.
[6] Z. Nisar, T. Hayat, A. Alsaedi, B. Ahmad, Significance of activation energy in radiative peristaltic transport of Eyring-Powell nanofluid, Int. Commun. Heat Mass Tran. 116 (2020), 104655.
[7] J.K. Madhukesh, R.N. Kumar, R.P. Gowda, B.C. Prasannakumara, G.K. Ramesh, M.I. Khan, Y.M. Chu, Numerical simulation of AA7072-AA7075/water-based hybrid nanofluid flow over a curved stretching sheet with Newtonian heating: a non-Fourier heat flux model approach, J. Mol. Liq. 335 (2021), 116103.
[8] Z. Nisar, T. Hayat, A. Alsaedi, S. Momani, Peristaltic flow of chemically reactive Carreau-Yasuda nanofluid with modified Darcy's expression, Mater. Today Commun. 33 (2022), 104532.
[9] M.I. Khan, S. Kadry, Y. Chu, M. Waqas, Modeling and numerical analysis of nanoliquid (titanium oxide, graphene oxide) flow viscous fluid with second order velocity slip and entropy generation, Chin. J. Chem. Eng. 31 (2021) 17–25.

[10] Z. Nisar, T. Hayat, K. Muhammad, B. Ahmed, A. Aziz, Significance of Joule heating for radiative peristaltic flow of couple stress magnetic nanofluid, J. Magn. Magn Mater. 581 (2021), 170951.
[11] U. Khan, N. Ahmed, S.T. Mohyud-Din, Y.M. Chu, I. Khan, K.S. Nisar, γ-Nanofluid thermal transport between parallel plates suspended by micro-cantilever sensor by incorporating the effective Prandtl model: applications to biological and medical sciences, Molecules 25 (2020) 1777.
[12] H. Yasmin, Z. Nisar, Mathematical analysis of mixed convective peristaltic flow for chemically reactive Casson nanofluid, Mathematics 11 (2023) 2673.
[13] P.J. Carreau, I.F. MacDonald, R.B. Bird, A nonlinear viscoelastic model for polymer solutions and melts-II, Chem. Eng. Sci. 23 (8) (1968) 901–911.
[14] T. Hayat, M. Waqas, S.A. Shehzad, A. Alsaedi, Stretched flow of Carreau nanofluid with convective boundary condition, Pramana 86 (2016) 3–17.
[15] M. Khan, M.Y. Malik, T. Salahuddin, I. Khan, Numerical modeling of Carreau fluid due to variable thicked surface, Results Phys. 7 (2017) 2384–2390.
[16] M. Waqas, M.I. Khan, T. Hayat, A. Alsaedi, Numerical simulation for magneto Carreau nanofluid model with thermal radiation: a revised model, Comput. Methods Appl. Mech. Eng. 324 (2017) 640–653.
[17] M.R. Eid, K.L. Mahny, T. Muhammad, M. Sheikholeslami, Numerical treatment for Carreau nanofluid flow over a porous nonlinear stretching surface, Results Phys. 8 (2018) 1185–1193.
[18] S.Z. Abbas, M. Waqas, A. Thaljaoui, M. Zubair, A. Riahi, Y.M. Chu, W.A. Khan, Modeling and analysis of unsteady second-grade nanofluid flow subject to mixed convection and thermal radiation, Soft Comput. 26 (2022) 1033–1042.
[19] M.S. Parvez, S. Reza-E-Rabbi, A. Al-Mamun, B.J. Rana, S.M. Arifuzzaman, M.S. Khan, MHD radiative Carreau-nanofluid stream through a plumb stretching sheet with the influence of binary chemical reaction and Arrhenius activation energy, AIP Conf. Proc. 2324 (2021), 040009.
[20] H. Waqas, M. Imran, M.M. Bhatti, Bioconvection aspects in non-Newtonian three-dimensional Carreau nanofluid flow with Cattaneo-Christov model and activation energy, Eur. Phys. J. Spec. Top. 230 (2021) 1317–1330.
[21] M. Akram, W. Jamshed, B.S. Goud, A.A. Pasha, T. Sajid, M.M. Rahman, M. Arshad, W. Weera, Irregular heat source impact on Carreau nanofluid flowing via exponential expanding cylinder: a thermal case study, Case Stud. Therm. Eng. 36 (2022), 102171.
[22] M. Ramzan, F. Ali, N. Akkurt, A. Saeed, P. Kumam, A.M. Galal, Computational Assessment of Carreau Ternary hybrid nanofluid influenced by MHD flow for Entropy generation, J. Magn. Magn Mater. 567 (2023), 170353.
[23] T. Hayat, Z. Nisar, A. Alsaedi, Bioconvection and Hall current analysis for peristalsis of nanofluid, Int. Commun. Heat Mass Tran. 129 (2021), 105693.
[24] M.M. Bhatti, S.R. Mishra, T. Abbas, M.M. Rashidi, A mathematical model of MHD nanofluid flow having gyrotactic microorganisms with thermal radiation and chemical reaction effects, Neural Comput. Appl. 30 (2018) 1237–1249.
[25] K. Ramesh, S.U. Khan, M. Jameel, M.I. Khan, Y.M. Chu, S. Kadry, Bioconvection assessment in Maxwell nanofluid configured by a Riga surface with nonlinear thermal radiation and activation energy, Surface. Interfac. 21 (2020), 100749.
[26] F. Haq, S. Kadry, Y.M. Chu, M. Khan, M.I. Khan, Modeling and theoretical analysis of gyrotactic microorganisms in radiated nanomaterial Williamson fluid with activation energy, J. Mater. Res. Technol. 9 (2020) 10468–10477.
[27] Y.M. Chu, M.I. Khan, H. Waqas, U. Farooq, S.U. Khan, M. Nazeer, Numerical simulation of squeezing flow Jeffrey nanofluid confined by two parallel disks with the help of chemical reaction: effects of activation energy and microorganisms, Int. J. Chem. React. Eng. 19 (2021) 717–725.
[28] T. Hayat, A. Alsaedi, B. Ahmad, Thermo-diffusion and diffusion-thermo impacts on bioconvection Walter-B nanomaterial involving gyrotactic microorganisms, Alex. Eng. J. 60 (2021) 5537–5545.
[29] A.J. Chamkha, H.A. Nabwey, Z.M.A. Abdelrahman, A.M. Rashad, Mixed bioconvective flow over a wedge in porous media drenched with a nanofluid, Journal of Nanofluids 8 (2019) 1692–1703.
[30] B.M.J. Rana, S.M. Arifuzzaman, S. Islam, S. Reza-E-Rabbi, A. Al-Mamun, M. Mazumder, K.C. Roy, M.S. Khan, Swimming of microbes in blood flow of nano-bioconvective Williamson fluid, Therm. Sci. Eng. Prog. 25 (2021), 101018.
[31] Z. Nisar, H. Yasmin, Analysis of motile gyrotactic micro-organisms for the bioconvection peristaltic flow of carreau–yasuda bionanomaterials, Coatings 13 (2023) 314.
[32] H. Waqas, U. Manzoor, M.S. Alqarni, T. Muhammad, Numerical Study for Bioconvection in Magnetized Flow of Micropolar Nanofluid Utilizing Gyrotactic Motile Microorganisms, Waves in Random and Complex Media, 2021, pp. 1–16.
[33] R.M. Muntazir, M. Mushtaq, K. Jabeen, A numerical study of MHD Carreau nanofluid flow with gyrotactic microorganisms over a plate, wedge, and stagnation point, Math. Probl Eng. 7 (2021) 1–22.
[34] A. Zaib, R.U. Haq, A.J. Chamkha, M.M. Rashidi, Impact of partial slip on mixed convective flow towards a Riga plate comprising micropolar TiO_2-kerosene/water nanoparticles, Int. J. Numer. Methods Heat Fluid Flow 29 (2019) 1647–1662.
[35] A. Gailitis, O. Lielausis, On a possibility to reduce the hydrodynamic resistance of a plate in an electrolyte, Appl. Magnetohydrodynamic 12 (1961) 143–146.
[36] T. Hayat, T. Abbas, M. Ayub, M. Farooq, A. Alsaedi, Flow of nanofluid due to convectively heated Riga plate with variable thickness, J. Mol. Liq. 222 (2016) 854–862.
[37] H. Vaidya, K.V. Prasad, I. Tlili, O.D. Makinde, C. Rajashekhar, S.U. Khan, R. Kumar, D.L. Mahendra, Mixed convective nanofluid flow over a non-linearly stretched Riga plate, Case Stud. Therm. Eng. 24 (2021), 100828.
[38] M. Rooman, M.A. Jan, Z. Shah, P. Kumam, A. Alshehri, Entropy optimization and heat transfer analysis in MHD Williamson nanofluid flow over a vertical Riga plate with nonlinear thermal radiation, Sci. Rep. 11 (2021) 1–14.
[39] P. Loganathan, K. Deepa, Stratified Casson fluid flow past a Riga-plate with generative/destructive heat energy, Int. J. Algorithm. Comput. Math. 6 (2020) 1–20.
[40] M.M. Bhatti, E.E. Michaelides, Study of Arrhenius activation energy on the thermo-bioconvection nanofluid flow over a Riga plate, J. Therm. Anal. Calorim. 143 (2021) 2029–2038.
[41] Q.H. Shi, A. Hamid, M.I. Khan, R.N. Kumar, R.J. Gowda, B.C. Prasannakumara, N.A. Shah, S.U. Khan, J.D. Chung, Numerical study of bio-convection flow of magneto-cross nanofluid containing gyrotactic microorganisms with activation energy, Sci. Rep. 11 (2021) 1–15.
[42] S. Hussain, S.M. Atif, M. Sagheer, M.A. Manzoor, MHD Carreau nanofluid with Arrhenius activation energy in porous medium, Sci. Iran. 29 (2022) 3591–3602.
[43] A. Shahid, M.M. Bhatti, R. Ellahi, K.S. Mekheimer, Numerical experiment to examine activation energy and bi-convection Carreau nanofluid flow on an upper paraboloid porous surface: application in solar energy, Sustain. Energy Technol. Assessments 52 (2022), 102029.
[44] B.M.J. Rana, S.M. Arifuzzaman, S. Islam, S. Reza-E-Rabbi, K.E. Hossain, S.F. Ahmmed, M.S. Khan, Swimming of microbes in entropy optimized nano-bioconvective flow of Prandtl-Erying fluid, Heat Transfer 51 (2022) 5497–5531.
[45] P.Y. Xiong, Y.M. Chu, M.I. Khan, S.A. Khan, S.Z. Abbas, Entropy optimized Darcy-Forchheimer flow of Reiner-Philippoff fluid with chemical reaction, Computational and Theoretical Chemistry 1200 (2021), 113222.
[46] M.M. Rashidi, N. Kavyani, S. Abelman, Investigation of entropy generation in MHD and slip flow over a rotating porous disk with variable properties, Int. J. Heat Mass Tran. 70 (2014) 892–917.
[47] T. Tayebi, H.F. Öztop, A.J. Chamkha, Natural convection and entropy production in hybrid nanofluid filled-annular elliptical cavity with internal heat generation or absorption, Therm. Sci. Eng. Prog. 19 (2020), 100605.
[48] Y.M. Chu, F. Shah, M.I. Khan, S. Kadry, Z. Abdelmalek, W.A. Khan, Cattaneo-Christov double diffusions (CCDD) in entropy optimized magnetized second grade nanofluid with variable thermal conductivity and mass diffusivity, J. Mater. Res. Technol. 9 (2020) 13977–13987.
[49] S. Mandal, G.C. Shit, S. Shaw, O.D. Makinde, Entropy analysis of thermo-solutal stratification of nanofluid flow containing gyrotactic microorganisms over an inclined radiative stretching cylinder, Therm. Sci. Eng. Prog. 34 (2022), 101379.
[50] S. Li, F. Ali, A. Zaib, K. Loganathan, S.M. Eldin, M. Ijaz Khan, Bioconvection effect in the Carreau nanofluid with Cattaneo–Christov heat flux using stagnation point flow in the entropy generation: micromachines level study, Open Phys. 21 (2023), 20220228.
[51] S.M. Arifuzzaman, M.S. Khan, M.S. Islam, M.M. Islam, B.M.J. Rana, P. Biswas, S.F. Ahmmed, MHD Maxwell fluid flow in presence of nano-particle through a vertical porous-plate with heat-generation, radiation absorption and chemical reaction, Heat Mass Tran. 9 (2017) 1–14.
[52] S. Reza-E-Rabbi, S.F. Ahmmed, S. Islam, S.M. Arifuzzaman, B.M.J. Rana, M.Y. Ali, A. Al-Mamun, M.S. Khan, Characterization of fluid flow and heat transfer of a periodic magnetohydrodynamics nano non-Newtonian liquid with Arrhenius activation energy and nonlinear radiation, Heat Transfer 51 (2022) 6578–6615.